IOP Publishing Physica Scripta
Phys. Scr. 95 (2020) 045202 (15pp) https://doi.org/10.1088/1402-4896/ab588e

A mathematical model of blood flow in a permeable channel: application to flat plate dialyzer

Muhammad Kahshan[1,2], Dianchen Lu[1,7], Mohammad Rahimi-Gorji[3,4] and Hoang-Thinh Do[5,6,7]

[1] Faculty of Science, Jiangsu University, Zhenjiang, Jiangsu 212013, People's Republic of China
[2] Department of Mathematics, COMSATS University Islamabad, Abbottabad Campus 22060, Pakistan
[3] Faculty of Medicine and Health Science, Ghent University, Ghent, B-9000, Belgium
[4] Biofluid, Tissue and Solid Mechanics for Medical Applications Lab (IBiTech- bioMMeda), Ghent University, Ghent, Belgium
[5] Division of Computational Mechatronics, Institute for Computational Science, Ton Duc Thang University, Ho Chi Minh City, Vietnam
[6] Faculty of Electrical & Electronics Engineering, Ton Duc Thang University, Ho Chi Minh City, Vietnam

E-mail: muhammadkahshan@gmail.com, dclu@ujs.edu.cn, mohammad.rahimigorji@ugent.be, m69.rahimi@yahoo.com and dohoangthinh@tdtu.edu.vn

Received 12 July 2019, revised 16 October 2019
Accepted for publication 18 November 2019
Published 11 February 2020

Abstract

This article presents the theoretical study of the physiological phenomenon brought up by filtration of a non-Newtonian Casson fluid between two parallel permeable membranes. This situation corresponds to blood filtration process in a flat plate hemodialyzer (FPH). Seepage of fluid across the membrane is considered in accordance with the Darcy's law and the equations of motion governing the flow are modeled. Using the low Reynolds number and long membrane length assumption, equations of motion are solved exactly. Equations describing velocity and pressure filed and various flow variables are derived and effects of wall slip parameter, wall filtration coefficient and the yield stress are presented graphically. A strong influence of these parameters is observed on the flow in an FPH. Theoretical values of the membrane filtration coefficient and mean pressure drop in an FPH are calculated and they are found to be in close agreement with the corresponding available empirical and experimental values in the literature. For certain limiting range of physical parameters, derived solutions reveal that the axial flow rate of Casson fluid in an FPH decays at an exponential rate. This is a physically valid and widely admitted result, used by several researchers in studying the blood filtration process in renal tubules of mammalian kidneys. Since the presented solutions in this article are reduced to their corresponding Newtonian fluid flow solutions between permeable membrane, therefore, it is concluded that a wide range of applications in physiology and engineering can be covered up by the present investigation.

Keywords: Casson fluid, permeable channel, non-Newtonian fluid, flat plate dialyzer, ultrafiltration rate

(Some figures may appear in colour only in the online journal)

1. Introduction

The study of fluid flow between parallel permeable membranes has scope in a wide area of science and engineering. This is encountered in biological and industrial processes of osmosis and ultra filtration For example, in reverse osmotic desalination, transpiration cooling, glomerular tubular ultra filtration, proximal tubular re-absorption, and in the process of blood filtration in an artificial kidney [1–5]. In these processes, the filtering fluid is normally pumped at an elevated

[7] Authors to whom any correspondence should be address.

pressure through porous-walled channels and tubes. For example, in the human body, the renal tubules of kidneys can be approximated by long narrow permeable tubes [2, 3, 5]. In the blood purification process in extra-corporeal circuits, the fluid commonly flows between flat parallel membranes composed of permeable materials [5, 6].

In studying hydrodynamics of flows in these processes, one must take into account normal and tangential components of the fluid velocity, in contrast to the flow in a confined region with impermeable boundaries. This is due to the fact that usual law proposed by Poiseuille [7] fails to be applicable in these flow phenomena. Berman's well known studies of laminar flows in permeable channels and tubes provide a starting point in the understanding of such flows [8, 9]. In these studies, he obtained approximate analytical solutions for velocity and pressure distribution for the steady motion of a linearly viscous and incompressible (Newtonian) fluid between permeable ducts having constant suction/injection velocity at their boundaries. A regular perturbation series approach was employed in obtaining solutions. Yuan *et al* investigated in detail the effect of constant suction and injection velocity on the steady flow of a Newtonian fluid in a permeable tube [10]. They considered a two-dimensional flow of incompressible Newtonian fluid in a porous-walled tube and presented approximate solution of equations of motion using the perturbation technique.

Macey [2, 3] investigated the hydrodynamics of flow of blood in the renal tubule of kidneys. In his investigations, Macey assumed the blood to be an incompressible Newtonian fluid and the renal tubule as a long narrow porous-walled tube. The flow rate of fluid was assumed to decay at a linear and exponential rates. Assuming the flow in renal tubule to be creeping, he obtained exact solutions for the velocity field and pressure distribution. Kozinski *et al* [6] extended the work of Macey for porous-walled channels and tubes composed of walls, reabsorbing the fluid at an exponentially decaying rate. In recent years, Haroon *et al* [11] proposed a mathematical model of fluid flow in renal tubules of kidneys. A two-dimensional model of creeping flow of Newtonian fluid in a permeable channel was proposed, where the fluid was assumed to be absorbed at a uniform rate. Siddiqui *et al* [12] presented the creeping flow of an incompressible Newtonian fluid in a permeable channel with linear seepage velocity at the wall. An application to renal tubular flow was also furnished.

Tu *et al* [13] developed a theoretical model for a two-dimensional flow of filtrate in a flat-plate dialyzer with the operation of ultra filtration In their study, they used the Crank–Nicolson technique to numerically solve the governing theoretical model. They also derived the fluid velocity profile and the concentration distribution in the dialysis system's membrane with the ultra filtration operation. The influences of channel thickness ratio, flow rates of retentate phase, dialysate phase and ultra filtration on the mass transfer rate and concentration distribution were studied. A considerable improvement in mass-transfer efficiency was gained with the employment of ultra filtration operation on the flat-plate dialyzer in comparison to the flat plate dialyzer without ultra filtration operation. They also performed an experiment that confirmed the accuracy of their proposed mathematical model. Zeng *et al* [14] studied the effect of permeability of membrane on the hydrodynamics in a parallel-plate co culture flow chamber (PPCFC). They demonstrated the membrane permeability as a function of membrane porosity, thickness, membrane shape and the membrane pore size. The commercial software Fluent was used to analyze the effect of membrane permeability on the hydrodynamics of flow in the PPCFC. Membrane permeability was found to be directly proportional to its thickness, porosity and the pore size whereas, it was found to be inversely proportional to the membrane surface shape factor. In the study of cells adhesion to a porous biomaterial, a new flow chamber was presented by Ghodsnia *et al* [15]. They studied the effect of trans-mural pressure and shear stress on cells adhesion to a porous biomaterial. Biochemical responses and morphology of cells that adhere to different biomaterials used in biochemical devices was also discussed due to the influence of induced forces.

However, in all articles enlisted in this literature review, (1) the fluid flowing in the channel was assumed to be Newtonian in nature, (2) the no-slip condition was assumed to be held at the permeable wall and (3) a seepage velocity of a constant, linear, or exponential type at the porous wall was assumed in advance. Most of the industrial and biological fluids are admitted to be non-Newtonian [16], and the classical Newton's law of viscosity fails to describe the complex rheological properties of these fluids. Among many existing constitutive models representing non-Newtonian fluids, the Casson fluid model is admitted to be a better and frequently-used model for physiological and biological fluids [17, 18]. One of the frequently used boundary condition in fluid mechanics problems is the no-slip condition. It states that the tangential velocity of the fluid layer in the region adjacent to boundaries has the same velocity as that of the boundary [7]. However, in many practical situations, this condition may fail to be valid, particularly when there are naturally permeable boundaries of the flow geometry [7, 19, 20]. A very thin layer of the fluid in the region adjacent to the permeable boundary slips, due to which a difference in the velocities of fluid layer and boundaries is encountered. Boundary conditions for a naturally-permeable wall, proposed by Beavers and Joseph [19] and slightly modified by Saffman [20], provide a mathematical form of the fluid slip phenomenon. In practical situations, seepage rates are normally determined by membrane characteristics and concentration polarization at the membrane surface and are not necessarily constant or known in advance.

Having the importance of physical aspects described, this article is aimed at studying the hydrodynamical aspects of the Casson fluid [17] in a porous-walled channel whose walls absorb the fluid at a variable rate in accordance with Darcy's law [21] and considering the wall slip effects. Thus, fluid seepage at the permeable wall of the channel is taken as a function of the difference of trans-mural pressure across the wall. Approach of the present article seems better than that adopted in [2, 3, 6, 11, 12] because: (1) the constitutive equation of the Casson fluid model can be reduced to the Newtonian fluid model as a special case when the yield stress

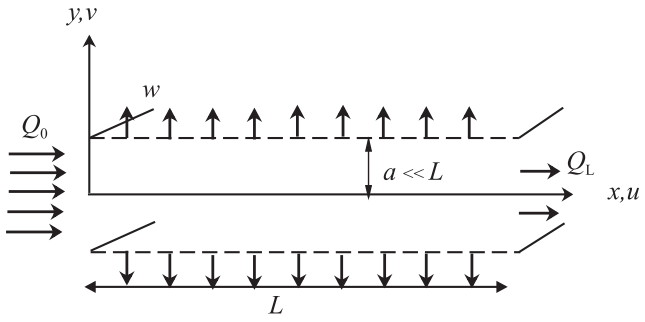

Figure 1. Geometry of the problem.

parameter in Casson model approaches to zero. Thus a larger class of biological and industrial fluids can be studied by using results of current investigation; (2) the Beavers and Josephs slip condition modified by Safffman [7, 19, 20] is applied at the membrane walls. When the slip parameter approaches to zero, results for the no-slip flow can be obtained from presented solutions in this article; (3) the obtained solution also reveals that for particular values of parameters, a uniform, linear, and exponentially-decaying flow rate can be deduced from the results of the current article, which were assumed in advance in the previous studies.

2. Mathematical model

A flat plat hemodialyzer (FPH) consists of several blood compartments. Each compartment comprises a pair of rectangular sheets made up of regenerated cellulose. The edges of each sheet are fastened by a pair of rectangular grooved plastic boards. The blood flows between the cellulose sheets, whereas the dialyzing fluid passes in a counter-current or a cross-current flow along the grooves in the hemodialyzer board [5, 22, 23].

We assume a single blood compartment of FPH to be a porous-walled channel of height $2a$, length L and width w. A cartesian coordinate system $(\bar{x}, \bar{y})$ is chosen such that $\bar{x}$-axis is the channel of symmetry and $\bar{y}$-axis is perpendicular to it as shown in figure 1. A two-dimensional, steady and creeping flow of an incompressible Casson fluid is considered in the channel such that the tangential and normal components of velocity are $\bar{u}(\bar{x}, \bar{y})$ and $\bar{v}(\bar{x}, \bar{y})$, respectively. The only deriving force for the fluid motion is assumed to be the fluids' hydrostatic pressure $\bar{p}(\bar{x}, \bar{y})$.

3. Nature of the fluid

Nature of the blood flowing in the FPH is assumed to be like Casson fluid, whose constitutive model is defined by

$$\sqrt{\bar{S}_{ij}} = \left[\sqrt{\mu} + \sqrt{\frac{\bar{S}_0}{|\bar{\mathbf{A}}_1|}}\right]^2 \sqrt{\bar{A}_{1_{ij}}} \quad \text{for } \bar{S} \geqslant \bar{S}_0, \tag{1}$$

$$|\bar{\mathbf{A}}_1| = 0 \text{ for } \bar{S} \leqslant \bar{S}_0, \tag{2}$$

where $\bar{\mathbf{A}}_1$ is the rate of strain tensor, $|\bar{\mathbf{A}}_1| = \sqrt{\frac{1}{2}\mathrm{tr}\bar{\mathbf{A}}_1^2}$, $\bar{S}$ is the magnitude of $\bar{\mathbf{S}}$, $\bar{S}_0$ is the yield stress and μ is the Casson's viscosity.

4. Equations of motion

Basic equations that govern the flow of an isotropic and incompressible fluid are momentum and the continuity equations [16]. For the flow under consideration, the momentum equation has the following component form

$$\rho\left(\bar{u}\frac{\partial \bar{u}}{\partial \bar{x}} + \bar{v}\frac{\partial \bar{u}}{\partial \bar{y}}\right) = -\frac{\partial \bar{p}}{\partial \bar{x}} + \frac{\partial \bar{S}_{\bar{x}\bar{x}}}{\partial \bar{x}} + \frac{\partial \bar{S}_{\bar{x}\bar{y}}}{\partial \bar{y}}, \tag{3}$$

$$\rho\left(\bar{u}\frac{\partial \bar{v}}{\partial \bar{x}} + \bar{v}\frac{\partial \bar{v}}{\partial \bar{y}}\right) = -\frac{\partial \bar{p}}{\partial \bar{y}} + \frac{\partial \bar{S}_{\bar{y}\bar{x}}}{\partial \bar{x}} + \frac{\partial \bar{S}_{\bar{y}\bar{y}}}{\partial \bar{y}}, \tag{4}$$

and the continuity equation is given by

$$\frac{\partial \bar{u}}{\partial \bar{x}} + \frac{\partial \bar{v}}{\partial \bar{y}} = 0, \tag{5}$$

where ρ is the fluid density and $\bar{S}_{\bar{x}\bar{x}}$, $\bar{S}_{\bar{x}\bar{y}}$, $\bar{S}_{\bar{y}\bar{x}}$ and $\bar{S}_{\bar{y}\bar{y}}$ are components of the stress tensor.

Following boundary conditions are imposed to complete the mathematical modeling of the described flow system:

slip boundary condition at the permeable wall of the dialyzer membrane :

$$\bar{u}(\bar{x}, a) = -\bar{\phi}\,\frac{\partial \bar{u}}{\partial \bar{y}}(\bar{x}, a), \tag{6}$$

seepage velocity at the membrane surface :

$$\bar{v}(\bar{x}, a, \bar{t}) = \frac{L_p}{\mu s}[\bar{p}(\bar{x}, a) - \bar{p}_m], \tag{7}$$

absence of transverse velocity in the plug flow region:

$$\bar{v}(\bar{x}, \bar{h}_p) = 0, \tag{8}$$

symmetry condition:

$$\frac{\partial \bar{u}}{\partial \bar{y}}(\bar{x}, \bar{h}_p) = 0, \tag{9}$$

mean inlet pressure and the inlet flow rate:

$$\bar{p}_i = \frac{1}{a - \bar{h}_p}\int_{\bar{h}_p}^{a} \bar{p}(0, \bar{y})\mathrm{d}\bar{y}, \tag{10}$$

$$\bar{Q}_0 = 2\,w\int_{\bar{h}_p}^{a} \bar{u}(0, \bar{y})\mathrm{d}\bar{y}. \tag{11}$$

In these equations $\bar{\phi}$ is the membrane slip coefficient usually measured in units of cm, L_p is the mechanical filtration coefficient of the membrane usually measured in the units of cm^2, μ is the fluid viscosity seeping through membrane, s is the membrane thickness, $\bar{h}_p$ is the height of the plug flow region, and $\bar{p}_m$ is the difference of the hydrostatic and osmotic pressure outside membrane. For further details of parameters and boundary conditions, authors refer the reader to [5, 19, 20, 24].

We now introduce the following variables to transform the problem into dimensionless form:

$$\left.\begin{aligned} &x = \frac{\bar{x}}{L},\ y = \frac{\bar{y}}{a},\ W = \frac{w}{a},\ u = \frac{a^2\bar{u}}{\bar{Q}_0},\\ &v = \frac{aL\bar{v}}{\bar{Q}_0},\ \lambda = \frac{a}{L},\ h_p = \frac{\bar{h}_p}{a},\ S = \frac{a^3\bar{S}}{\mu\bar{Q}_0},\\ &S_0 = \frac{a^3\bar{S}_0}{\mu\bar{Q}_0},\ \phi = \frac{\bar{\phi}}{a},\ p = \frac{a^4[\bar{p} - \bar{p}_m]}{\mu L\bar{Q}_0},\\ &Q = \frac{\bar{Q}}{\bar{Q}_0},\ Re = \frac{\rho\bar{Q}_0}{\mu L},\ K = \frac{L_pL^2}{a^3\, s}, \end{aligned}\right\}, \tag{12}$$

where K is the dimensionless filtration coefficient of the membrane, ϕ is the dimensionless slip coefficient of the membrane, λ is the ratio of half channel height to its length, S_0 is the dimensionless yield stress and Re denotes the Reynolds number.

Since for the flow in FPH, the parameter λ and the Reynolds number are small [5, 25, 26], therefore, it is reasonable to ignore terms of the order λ^2 and Re. Smallness of λ and Re will also be shown in the coming section. Thus, using the low Reynold number and small λ assumptions, equations (3)–(5)) reduce to the following form:

$$\frac{\partial p}{\partial x} = \frac{\partial S_{xy}}{\partial y}, \tag{13}$$

$$\frac{\partial p}{\partial y} = 0, \tag{14}$$

$$\frac{\partial u}{\partial x} + \frac{\partial v}{\partial y} = 0. \tag{15}$$

The constitutive equations (1) and (2) of the Casson fluid result in:

$$\sqrt{S_{xy}} = \sqrt{S_0} + \sqrt{\frac{\partial u}{\partial y}} \text{ for } S \geqslant S_0, \tag{16}$$

$$\frac{\partial u}{\partial y} = 0 \text{ for } S \leqslant S_0. \tag{17}$$

The boundary conditions (6)–(11) are transformed into the following dimensionless form:

$$u(x, 1) = -\phi\,\frac{\partial u}{\partial y}(x, 1), \tag{18}$$

$$v(x, 1) = Kp(x, 1), \tag{19}$$

$$v(x, h_p) = 0, \tag{20}$$

$$\frac{\partial u}{\partial y}(x, h_p) = 0, \tag{21}$$

$$p_i = \frac{1}{1 - h_p}\int_{h_p}^{1} p(0, y)\mathrm{d}y, \tag{22}$$

$$1 = 2W\int_{h_p}^{1} u(0, y)\mathrm{d}y. \tag{23}$$

The height h_p of plug flow region can be computed from equations (13), (14) and (16) as:

$$h_p = S_0 \Big/ \frac{\partial p}{\partial x}. \tag{24}$$

5. Solution

Integrating equation (13) once with respect to y along with equation (14), we get

$$S_{xy} = \frac{\mathrm{d}p}{\mathrm{d}x}y + f_1(x), \tag{25}$$

where $f_1(x)$ is a function of x.

Using equation (25) in (13) along with the boundary condition (21) we obtain

$$\frac{\partial u}{\partial y} = \frac{\mathrm{d}p}{\mathrm{d}x}(y - 2\sqrt{h_p y} + h_p). \tag{26}$$

Finally, integrating equation (26) with respect to y from y to h_p, and using the slip condition (21) we obtain the tangential component of the velocity field as follows:

For $h_p \leqslant y \leqslant 1$:

$$u(x, y) = \frac{1}{6}\frac{\mathrm{d}p}{\mathrm{d}x}[3(y^2 - 1 - 2\phi) - 4\sqrt{h_p}(2\sqrt{y^3} - 2 - 3\phi) + 6h_p(y - 1 - \phi)]. \tag{27}$$

By substituting $y = h_p$ in equation (27), the plug flow velocity $u_p(x)$ can be readily obtained as follows:

For $0 \leqslant y \leqslant h_p$:

$$u_p(x) = \frac{1}{6}\frac{\mathrm{d}p}{\mathrm{d}x}[3(h_p^2 - 1 - 2\phi) - 4\sqrt{h_p}(2\sqrt{h_p^3} - 2 - 3\phi) + 6h_p(h_p - 1 - \phi)]. \tag{28}$$

Solving equation of continuity and employing the boundary condition (20), the transverse component of the velocity field can be obtained as follows:

For $h_p \leqslant y \leqslant 1$:

$$\begin{aligned} v(x, y) = -\frac{1}{30}\frac{\mathrm{d}^2p}{\mathrm{d}x^2}[5\{(y^3 - 3y - 6\phi y) - (h_p^3 - 3h_p - 6\phi h_p)\} - 4\sqrt{h_p}\{(4\sqrt{y^5} - 10y - 15\phi y) - (4\sqrt{h_p^5} - 10h_p - 15\phi h_p)\} + 15h_p\{(y^2 - 2y - 2\phi y) - (h_p^2 - 2h_p - 2\phi h_p)\}]. \end{aligned} \tag{29}$$

Note that the transverse velocity in the plug flow region is zero as can be sen from equation (20).

Evaluating $v(x, y)$ at the wall and employing the boundary condition (19) we obtain the following differential equation for the pressure distribution of fluid in the channel:

$$\frac{\mathrm{d}^2 p}{\mathrm{d}x^2} - \frac{6\,K}{\lambda_1} p = 0, \tag{30}$$

where

$$\lambda_1 = (2 + 2\phi) + (h_p^3 - 3h_p - 2h_p\phi) - \frac{4}{5}h_p\{(6 + 15\phi) + (4\sqrt{h_p^5} - 10h_p - 15\phi h_p)\} + 3h_p\{(1 + 2\phi) + (h_p^2 - 2h_p - 2\phi h_p)\}. \tag{31}$$

Exact solution of equation (30) along with the inlet conditions (22) and (23) is given as follows:

$$p(x) = p_i \cosh \zeta x - \frac{\zeta}{2\,W\,K} \sinh \zeta x, \tag{32}$$

where $\zeta = \sqrt{\frac{6\,K}{\lambda_1}}$.

Equation for dimensionless mean pressure $P_M(x)$ can be computed by the following relation

$$\begin{aligned} P_M(x) &= \int_0^{h_p} p(x, y)\mathrm{d}y + \int_{h_p}^1 p(x, y)\mathrm{d}y, \\ &= p(x), \\ &= p_i \cosh \zeta x - \frac{\zeta}{2\,W\,K} \sinh \zeta x. \end{aligned} \tag{33}$$

The mean pressure difference of the Casson fluid between the channel entrance region and arbitrary point x_k is given by the expression

$$\begin{aligned} \triangle p(x_k) &= P_M(0) - P_M(x_k), \\ &= p_i(1 - \cosh \zeta\, x_k) + \frac{\zeta}{2\,W\,K} \sinh \zeta\, x_k. \end{aligned} \tag{34}$$

The local wall shear stress can be readily computed from equations (26) and (32) as follows

$$\begin{aligned} \tau_w &= -S_{xy}|_{y=1}, \\ &= -\frac{\partial u}{\partial y}|_{y=1}, \\ &= -(1 - 2\sqrt{h_p} + h_p)\left(p_i\,\zeta \sinh \zeta x - \frac{\zeta^2}{2\,W\,K} \cosh \zeta x\right). \end{aligned} \tag{35}$$

Using equation (32) in (24), yield stress for the casson fluid can be obtained as

$$S_0 = h_p\, p_i\, \zeta \sinh \zeta\, x - \frac{h_p\, \zeta^2}{2\,W\,K} \cosh \zeta x. \tag{36}$$

The volume flow rate for the Casson fluid is defined as

$$Q(x) = 2W\left(\int_0^{h_p} u_p(x)\mathrm{d}y + \int_{h_p}^1 u(x, y)\mathrm{d}y\right), \tag{37}$$

which, in view of equations (27) and (28) becomes

$$Q(x) = p_i\, W\, \zeta\, \lambda_2\left(\frac{\zeta}{2p_i\, W\, K} \cosh \zeta\, x - \sinh \zeta\, x\right), \tag{38}$$

where

$$\lambda_2 = \frac{2}{3}(1 + \phi) - \frac{4}{5}(2 + 5\phi)\sqrt{h_p} + (1 + 2\phi)h_p - (1 + 3\phi)h_p^2 - \frac{22}{5}h_p^3. \tag{39}$$

Stream function $\psi(x, y)$ can be evaluated by the following equation

$$\mathrm{d}\psi = u\,\mathrm{d}x - v\,\mathrm{d}y. \tag{40}$$

Using equations (27) and (29) in conjunction with (32), we obtain the following expression for the stream function

$$\psi(x, y) = [5(y^3 - 3y - 6\phi y) - 4\sqrt{h_p}(4\sqrt{y^5} - 10y - 15\phi y) + 15h_p(y^2 - 2y - 2\phi y)] \times \left(p_i\,\zeta \sinh \zeta\, x - \frac{\zeta^2}{2p_i\, W\, K} \cosh \zeta\, x\right). \tag{41}$$

In the limiting case, when $\phi \to 0$, solutions presented in equations (27), (29), (32), (35), (38) and (41) correspond to the no-slip flow of a Casson fluid in a permeable channel. When $\phi \to 0$ and $h_p \to 0$ the obtained solutions correspond to the Newtonian fluid flow solutions in a permeable channel as a special case. For example, a result relating mean pressure and the flow rate can be obtained from equations (33) and (38), namely

$$\frac{\mathrm{d}P_M}{\mathrm{d}x} = -\Gamma_c\, Q(x), \tag{42}$$

where

$$\Gamma_c = \frac{1}{\lambda_2\, W}. \tag{43}$$

The corresponding analogous law that relates the volumetric flow rate and the pressure gradient resulting for the flow of laminar flow of incompressible Newtonian fluid between non-porous parallel flat plates. However, in that case

$$\frac{\mathrm{d}P_M}{\mathrm{d}x} = -\Gamma_N\, Q(x), \tag{44}$$

where

$$\Gamma_N = \frac{3\,\mu}{2\,w\,a^3}. \tag{45}$$

Equation (44) can be deduced from (42) as a special case by substituting dimensionless parameters defined in (12) and $(\phi, h_p) \to (0, 0)$ in (44) along with (43) and (39).

6. Graphs and discussion

In this section, we present graphical behavior of velocity field, streamline pattern ad the mean pressure drop with the variations of yield stress parameter h_p (or the height of the plug

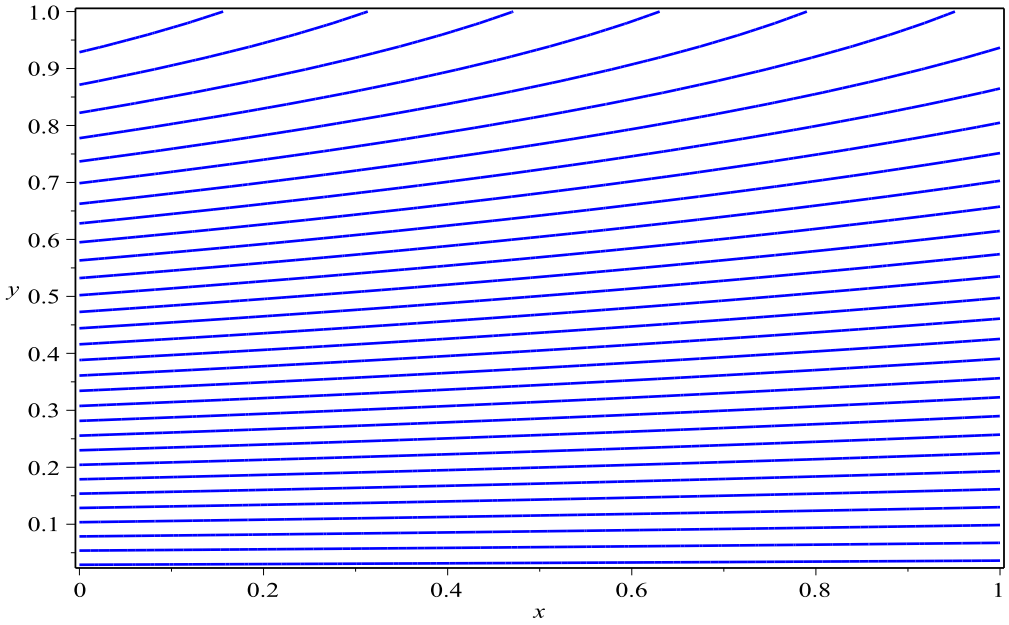

Figure 2. Streamline pattern for $p_i = 0.02$, $K = 0.004$, $\phi = 0.2$, $h_p = 0.005$, $W = 1288$.

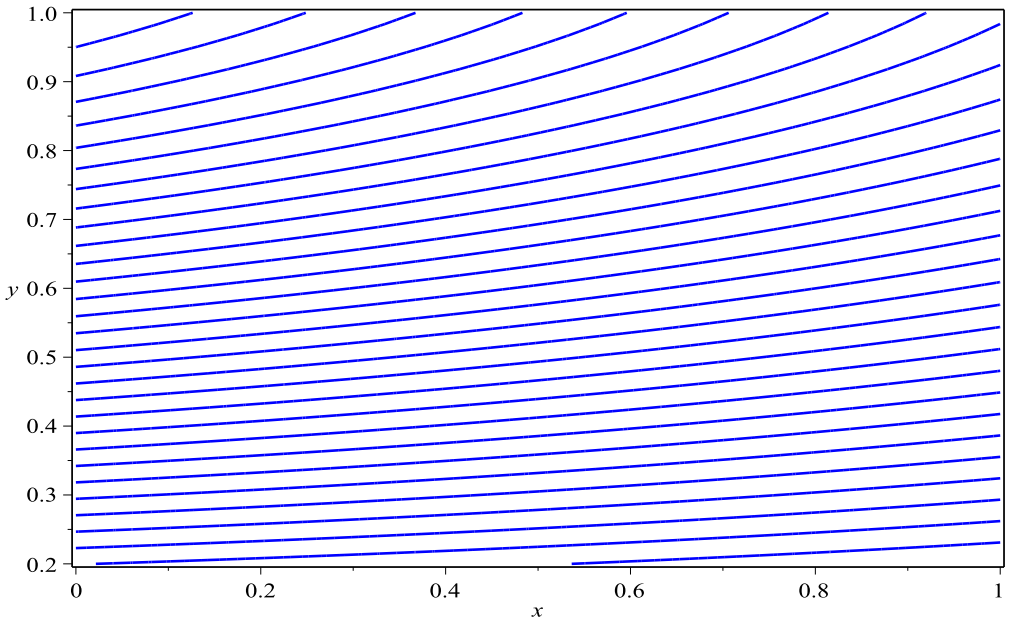

Figure 3. Streamline pattern for $p_i = 0.02$, $K = 0.004$, $\phi = 0.2$, $h_p = 0.3$, $W = 1288$.

flow region), wall slip parameter ϕ and the membrane filtration coefficient K. All graphs are plotted in the region where $h_p \leqslant y \leqslant 1$, and $(U, V, P) = 10^3(u, v, \triangle p)$.

Streamlines of the flow are plotted in figures 2–4. Figure 2 shows that for certain values of parameters, the flow is forward and positive along the membrane length. No reverse flow and leakage is observed in this figure due to the moderate values of all parameters. Figure 3 is plotted to study effect of yield stress parameter on the flow field. The fluid seepage through membrane surface is seen to be increased for a higher magnitude of the yield stress parameter. This is due to the fact that higher magnitudes of h_p produce high pressure gradients in the flow (it can be observed in figure 11) and consequently the seepage is seen to be increased. Effect of membrane filtration coefficient on the flow pattern is shown in figure 4. It is observed that by increasing the membrane permeability, fluid absorption rate is increased. For higher values of membrane permeability, a stagnation point flow can also be seen in this figure. This phenomenon also strengthens the validity of presented solutions because for membranes with higher permeability, the pore size/membrane structure allows more fluid to pass through it and hence the fluid absorption is expected to increase. These figures also help us understanding the mechanism of membrane filtration process,

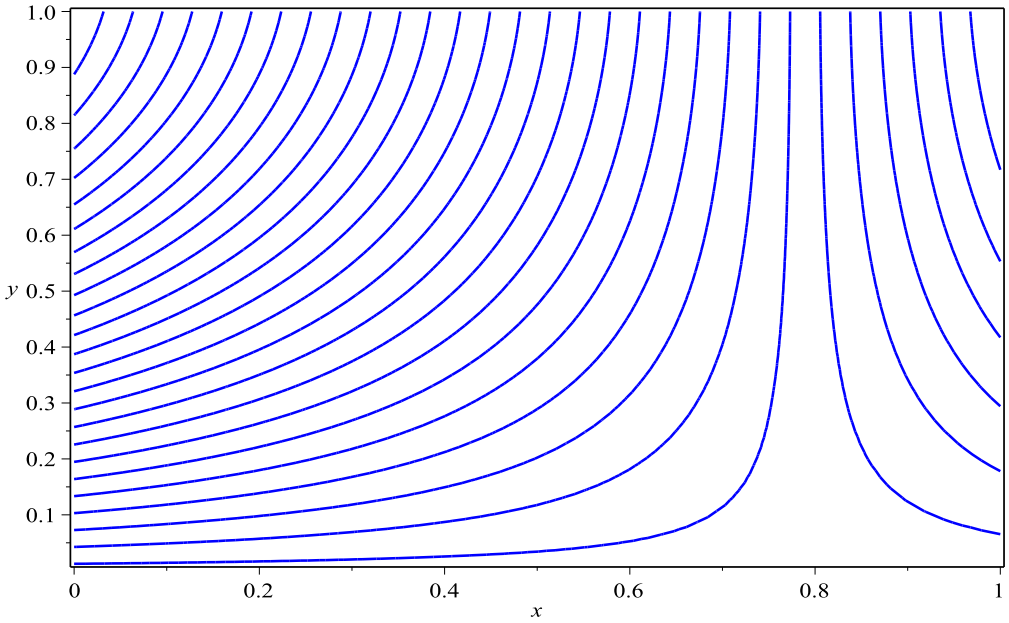

Figure 4. Streamline pattern for $p_i = 0.02$, $K = 0.025$, $\phi = 0.3$, $h_p = 0.005$, $W = 1288$.

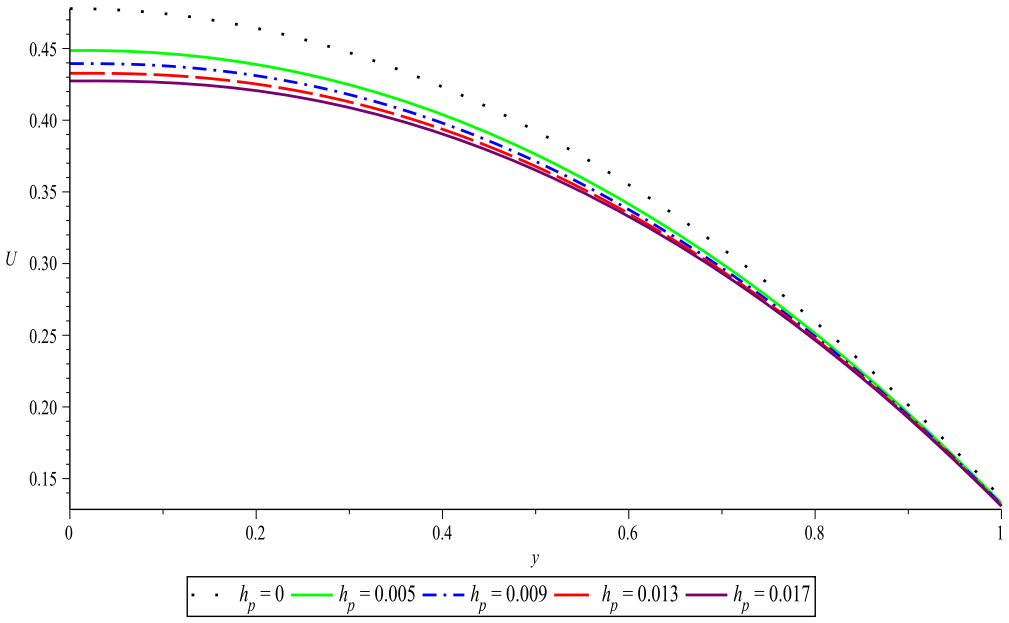

Figure 5. Variation of axial velocity with yield stress, $p_i = 0.02$, $K = 0.025$, $\phi = 0.2$, $W = 1288$.

and it can be sought that for physiological and biological flows in which the reverse flow is not admissible, one should chose a membrane within a specified permeability range. And also for filtration of fluids with higher yield stresses, one should take the high seepage into account in advance.

Variations in the axial and normal velocity profiles with the yield stress parameter are plotted in figures 5 and 6 at the cross section $x = 0.3$ of the channel. In these figures, the black dotted lines correspond to the Newtonian fluid flow profiles. A deviation in the axial and normal velocity components from that of Newtonian fluid can be seen in these figures due to the different constitutive relations of both fluid models and physical properties. These figures reveal that the magnitudes of both velocity components are decreased with the increase in height of the plug flow region. Another aspect of increasing h_p is the fluid tendency from Newtonian to non-Newtonian behavior. Thus we observe a damping in both velocity components due to non-Newtonian nature of the Casson fluid. Variations of velocity components with increasing the membrane permeability are drawn in figures 7 and 8. Magnitude of the axial velocity component is seen to decrease with the increasing values of K. It happened because of the fact that an increase in membrane permeability causes higher amount of fluid to be filtered through membrane surface in the normal direction, and consequently the magnitude of axial velocity is seen to decrease. Effect of membrane

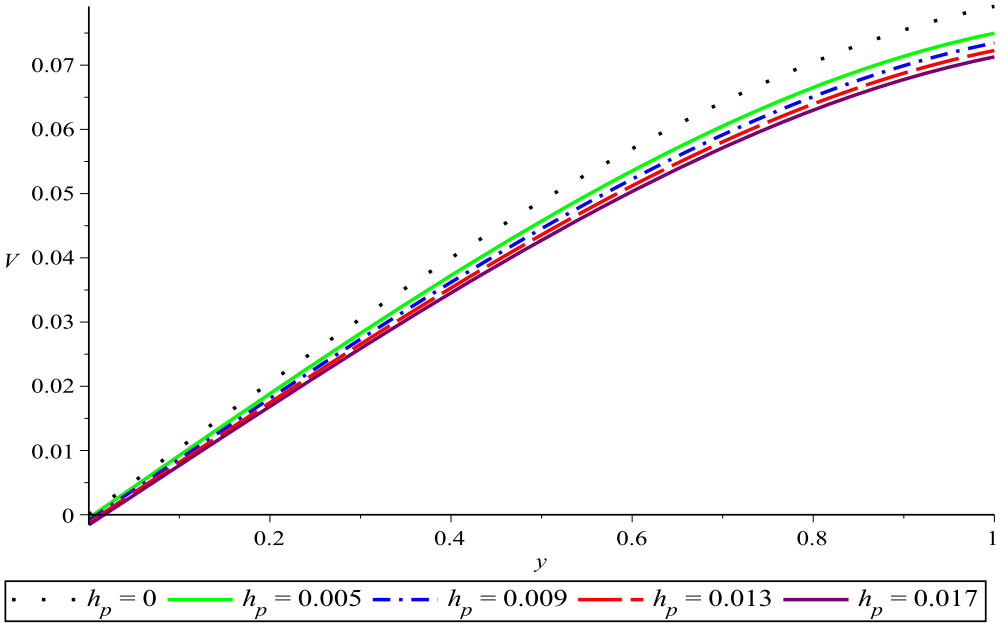

Figure 6. Variation of normal velocity with yield stress, $p_i = 0.02$, $K = 0.025$, $\phi = 0.2$, $W = 1288$.

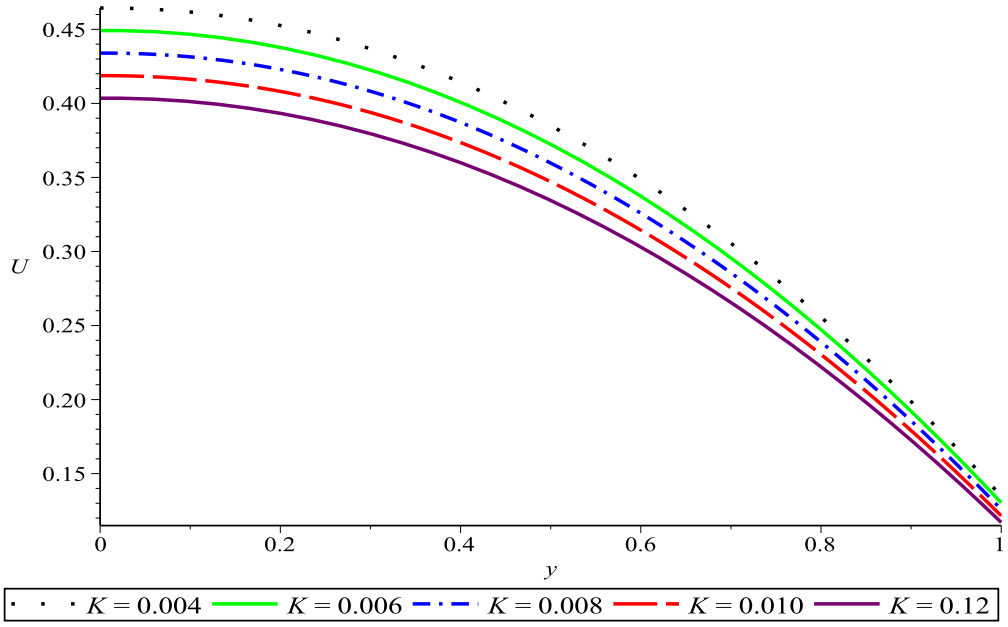

Figure 7. Variation of tangential velocity with membrane filtration coefficient, $p_i = 0.02$, $\phi = 0.2$, $h_p = 0.001$, $W = 1288$.

permeability coefficient on the normal component of the velocity field is opposite to that on the axial component. It is happening since the flow field has both non zero tangential and normal velocity components. An increase in the magnitude of normal component with K weakens the axial velocity U and vice versa. From figure 8 it is noted that the magnitude of the transverse velocity component increases rapidly as the membrane filtration coefficient is increased. This effect is similar to that observed in the streamline pattern in figure 4 where fluid filtration through membrane was observed higher for higher magnitude of K and was explained in the preceding paragraph.

Impact of the dimensionless membrane slip coefficient ϕ on velocity components is plotted in figures 9 and 10. In these figures, the black dotted lines correspond to the velocity components for no slip flow of the Casson fluid in a permeable channel. Effect of wall slip parameter is clearly visible in these two figures. The tangential velocity initially decreases in the region near inlet by increasing the wall slip parameter, then a point $y = y_0$ can be seen where the axial velocity is invariant of the magnitude of ϕ. After the point $y = y_0$, axial velocity starts increasing with the increasing values of membrane slip coefficient. The slip boundary condition states that a thin fluid layer adjacent to membrane surface exists that

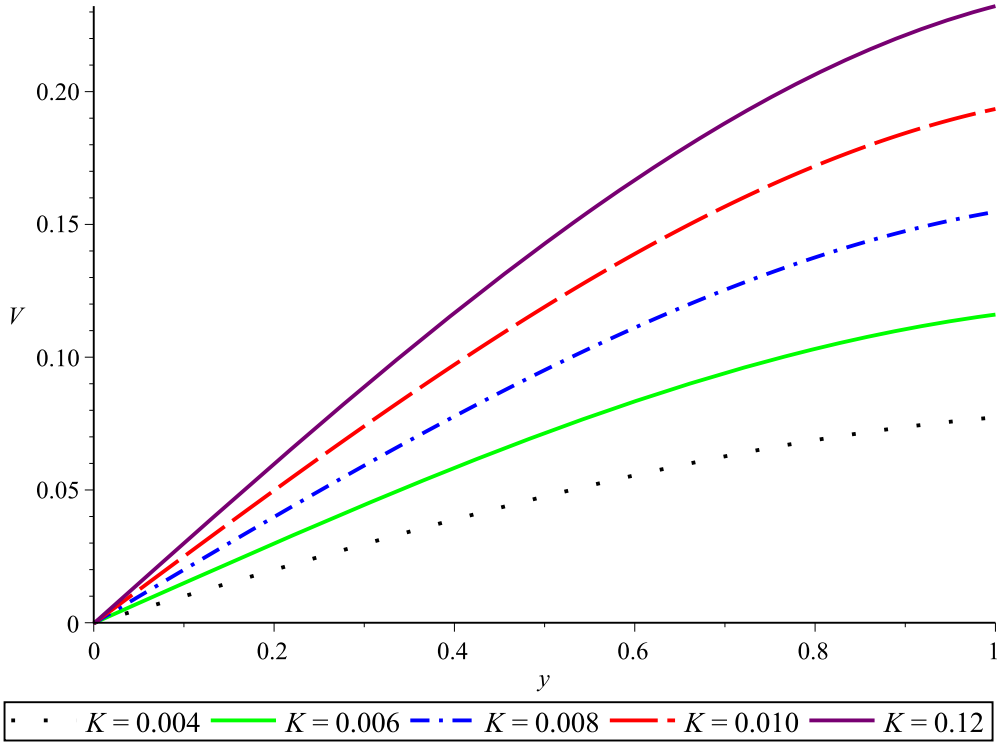

Figure 8. Variation of normal velocity with membrane filtration coefficient, $p_i = 0.02$, $\phi = 0.2$, $h_p = 0.001$, $W = 1288$.

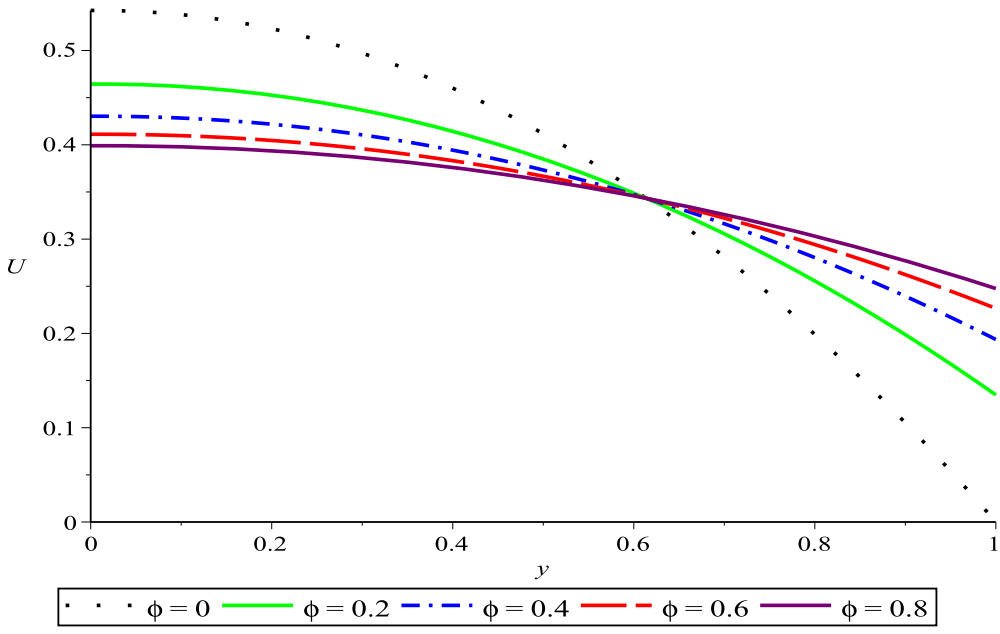

Figure 9. Variation of tangential velocity with wall slip coefficient, $p_i = 0.02$, $K = 0.004$, $h_p = 0.001$, $W = 1288$.

has a slip velocity u_s whose magnitude is proportional to the velocity gradient at the membrane surface (with constant of proportionality ϕ), in contrast to the usual no slip flow where the fluid at the membrane wall has zero velocity [7]. This effect is noticed in figure 9 where the tangential velocity has a non-zero value at the membrane wall, and for higher slip coefficient it has higher magnitude. In the region away from the membrane surface and closer to the center line, this impact is reversed due to the regularity condition (9). This impact of slip parameter on the axial velocity is qualitatively same as observed by Hayat *et al* [27] and Tripathi [28]. Figure 10 reveals that magnitude of the transverse component of velocity decreases as the membrane slip coefficient is increased. However this increase in normal velocity is quantitatively very smaller than the impact of slip parameter on the axial velocity component.

Variations of mean trans-mural pressure difference between membranes are sketched in figures 11 and 12. It is

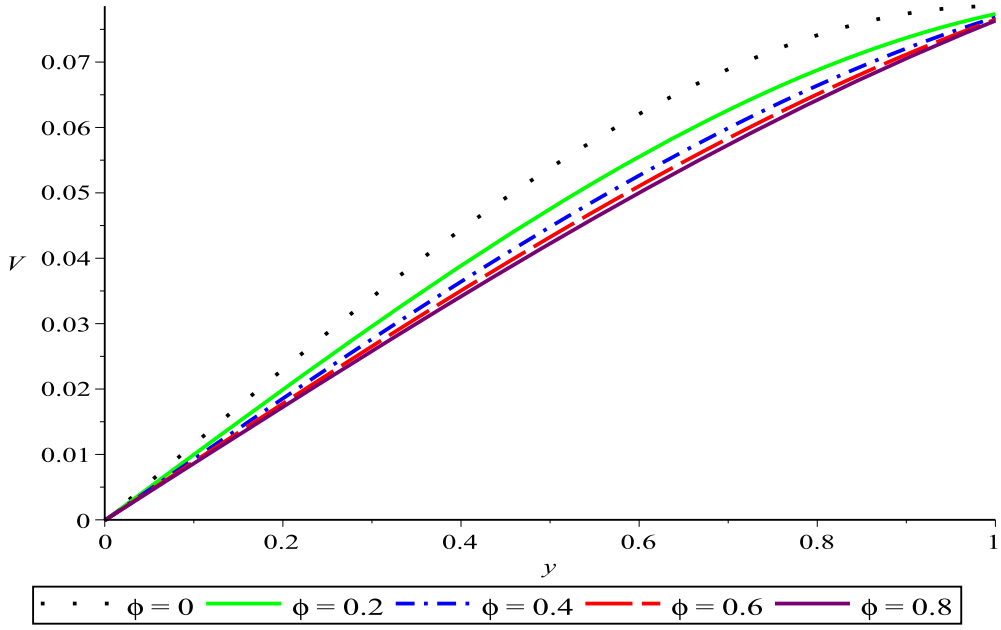

Figure 10. Variation of normal velocity with wall slip coefficient, $p_i = 0.02$, $K = 0.004$, $h_p = 0.001$, $W = 1288$.

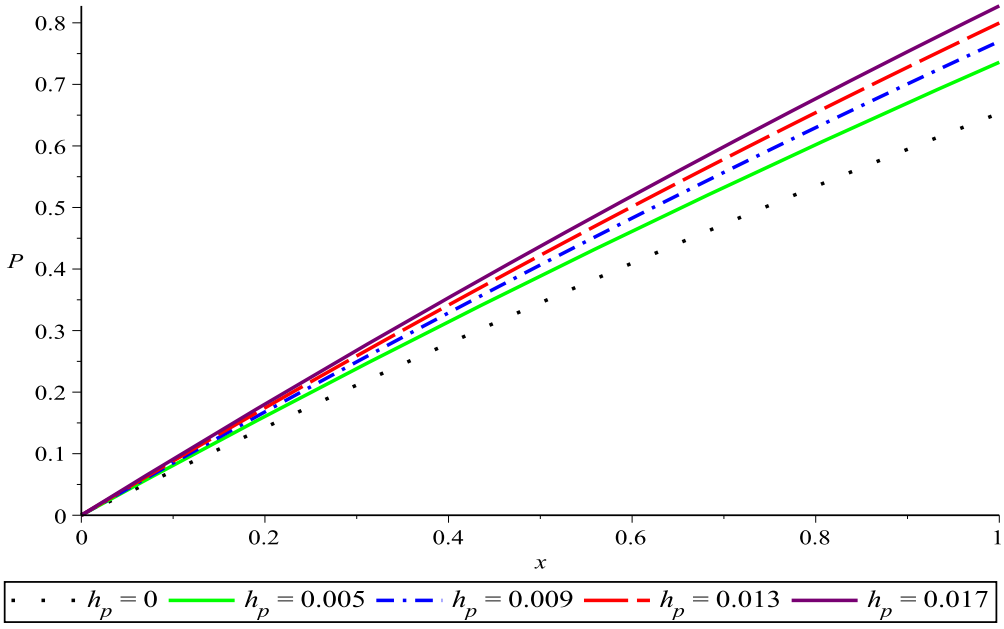

Figure 11. Variation of mean pressure drop with yield stress, $p_i = 0.02$, $K = 0.025$, $\phi = 0.2$, $W = 1288$.

observed from figure 11 that the magnitude of mean pressure drop is higher for Casson fluid than that of Newtonian fluid in permeable channel. By increasing the height of plug flow region h_p, mean pressure difference is observed to increase rapidly and vice versa. For an increased yield stress, the domain of flow regime $0 \leqslant h_p \leqslant y \leqslant 1$ is reduced, that causes the increased mean pressure drop. Here we also note that increasing the magnitude of h_p shows the fluid tendency towards non-Newtonian behavior. Thus, an increased mean pressure drop is faced for non-Newtonian fluid flow in comparison to the Newtonian fluid. This observation was also pointed out by study of Pandey *et al* [29] for the flow of concentrated fluid in esophagus. Impact of dimensionless membrane filtration coefficient K on P is plotted in figure 12. It is found that mean pressure drop decays with the higher values of filtration coefficient. This effect is qualitatively opposite to that due to increase in h_p. Since for a given volume of fluid, higher membrane permeability implies more fluid absorption through membrane surface, which in turns reduces the mean pressure drop.

Behavior of local wall shear stress with the variations of yield stress and the filtration coefficient is presented in

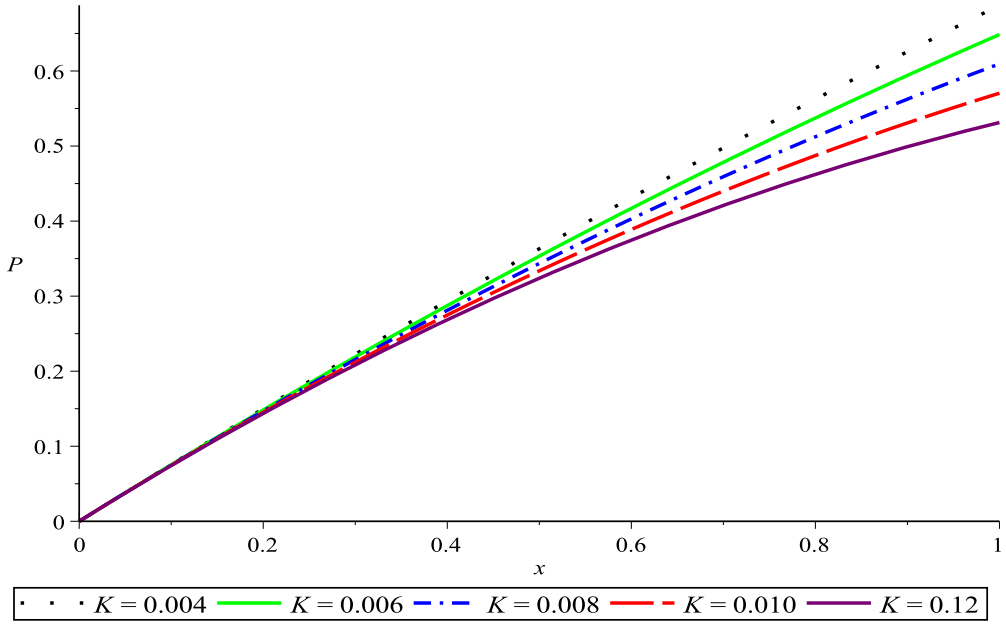

Figure 12. Variation of mean pressure drop with membrane filtration coefficient, $p_i = 0.02$, $\phi = 0.2$, $h_p = 0.001$, $W = 1288$.

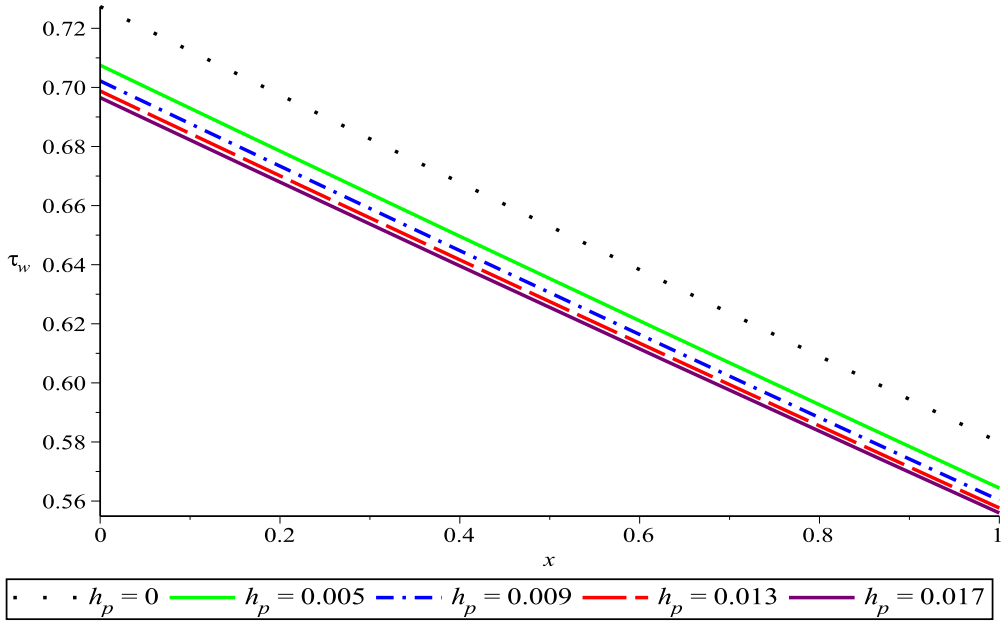

Figure 13. Variation of wall shear stress with yield stress, $p_i = 0.02$, $K = 0.025$, $\phi = 0.2$, $W = 1288$.

figures 13 and 14. It is observed from both of these figures that wall shear stress decreases as the magnitude of yield stress and filtration coefficient of membrane are increased and vice versa. Since by having increase in the yield stress, width of the core region widens and more fluid moves with a constant velocity u_p, therefore the local wall shear stress is found to be decreased. Similarly, when the membrane permeability increases, the fluid leakage enhances which results in the reduced local wall shear stress. A similar behavior in the profile of wall shear stress was also observed by Bigyani *et al* in the study of blood flow in arteriosclerosis [30].

7. Application to FPH

This section is devoted to theoretical expressions and numerical calculations for the ultrafiltration rate and mean pressure drop in the axial direction in and FPH. As described in section 2, an FPH comprises of a number of blood compartments. Each of these compartment contains a pair of rectangular sheets which are made up of regenerated cellulose. Sheets are inserted in a pair of rectangular grooved plastic boards at their edges.The filtering blood is passed to flow between the cellulose sheets. Meanwhile, a dialyzing fluid is passed to flow in the grooves in the hemodialyzer

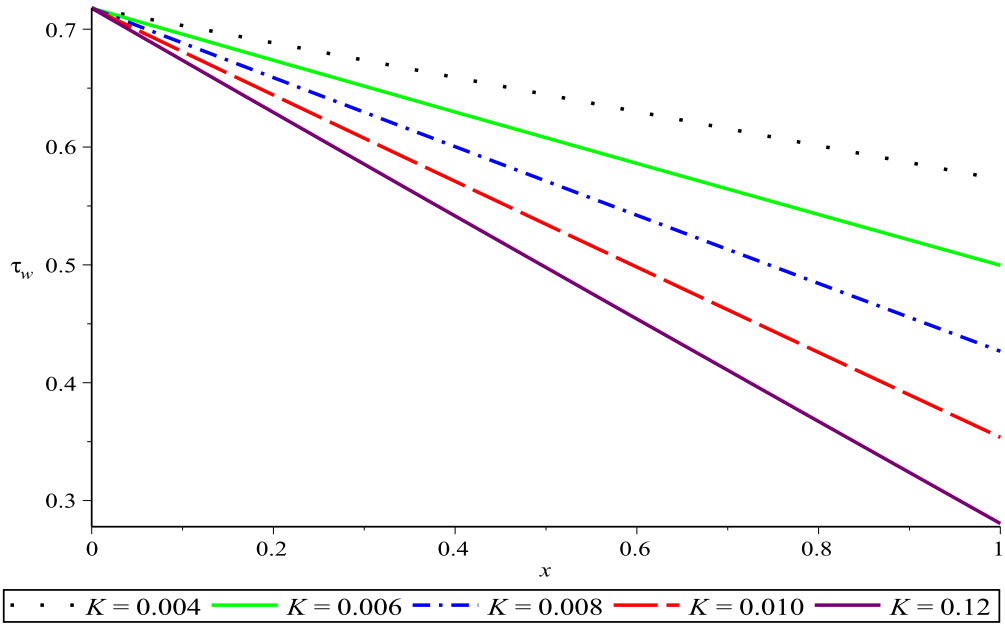

Figure 14. Variation of wall shear stress with membrane filtration coefficient, $p_i = 0.02$, $\phi = 0.2$, $h_p = 0.001$, $W = 1288$.

board in a counter-current or a cross-current way [5, 22, 23]. In a given time, the amount of blood volume lost by leakage through the cellulose from a known recirculating volume, is called the ultrafiltration rate.

If L is the length of cellulose, then the ultrafiltration rate for the presented model is given as:

$$\bar{Q}_U = \bar{Q}_0 - \bar{Q}_L, \tag{46}$$

where $\bar{Q}_0$ and $\bar{Q}_L$ denote the dimensional flow rates at he inlet and exit of the FPH, respectively. Expression for the dimensionless ultrafiltration rate can be obtained using parameters defined in (12). This yields

$$\begin{aligned} Q_U &= Q(0) - Q(1), \\ &= 3\,\lambda_3\left[1 - \cosh\zeta + \frac{2p_i\,W\,K}{\zeta}\sinh\zeta\right], \end{aligned} \tag{47}$$

where $\lambda_3 = \dfrac{\lambda_2}{\lambda_1}$.

The expression for mean pressure drop in the axial direction between $x = 0$ and $x = L$ can also be obtained in a similar manner. By using equation (34), we have the following expression for the mean pressure drop in a FPH:

$$\begin{aligned} \triangle p(1) &= p(0) - p(1), \\ &= p_i\left[1 - \cosh\zeta + \frac{\zeta}{2p_i\,W\,K}\sinh\zeta\right]. \end{aligned} \tag{48}$$

In order to check the accuracy of the presented formulas, exact values of the involved parameters corresponding to the FPH are needed. For this purpose, we have used the experimental data provided in [5, 23] corresponding to a flat-plate disposable artificial kidney, referred to as RP kidney. This data is given in table 1. For yield stress and slip parameter values, we have utilized results of [25, 31]. From the data in table 1, we found that the parameter λ is of order 10^{-8}.

Table 1. Physiological data related to the RP kidney [4, 23].

Parameter	Abbreviation	Numerical value
Number of blood compartments		8
Membrane length	L	42 cm
Membrane width	w	11.6 cm
Membrane thickness	t	2.59×10^{-3} cm
Blood half channel height	a	9×10^{-3} cm
Fluid viscosity	μ	6.9×10^{-3} dynes s cm^{-2}
Transmembrane pressure difference at the entrance	$\bar{p}_i - P_T$	150 mm Hg
Total ultrafiltration rate	$8\bar{Q}_w$	200 ml h^{-1}
Total entrance volume flow rate	$8\bar{Q}_0$	160 ml min^{-1}

Therefore, ignoring terms of the order λ^2 is justified for the flow in a flat plate dialyzer. By making use of these parameters along with $\phi = 0.1$ and $h_p = 0.001$ in equation (47), an algebraic equation in one variable K is obtained. By expanding terms in the power series of K up to $O(K^5)$ and solving the resulting equation, we obtain a real root of this equation as $K = 0.0005$. The magnitude of the ultrafiltration coefficient L_p was then calculated from $K = \dfrac{L_p L^2}{a^3 t}$. This resulted in $L_p = 5.35 \times 10^{-16}\,\text{cm}^2$. In a similar way and adopting the same steps, equation (48) results in the value of mean pressure drop in a FPH as 10.39 mm Hg.

The value of the filtration coefficient L_p is usually not given in the data for membranes of hemodialyzers. The result of experiments performed by Kaufmann *et al* [32] show that at the normal body temperature, regenerated cellulose has

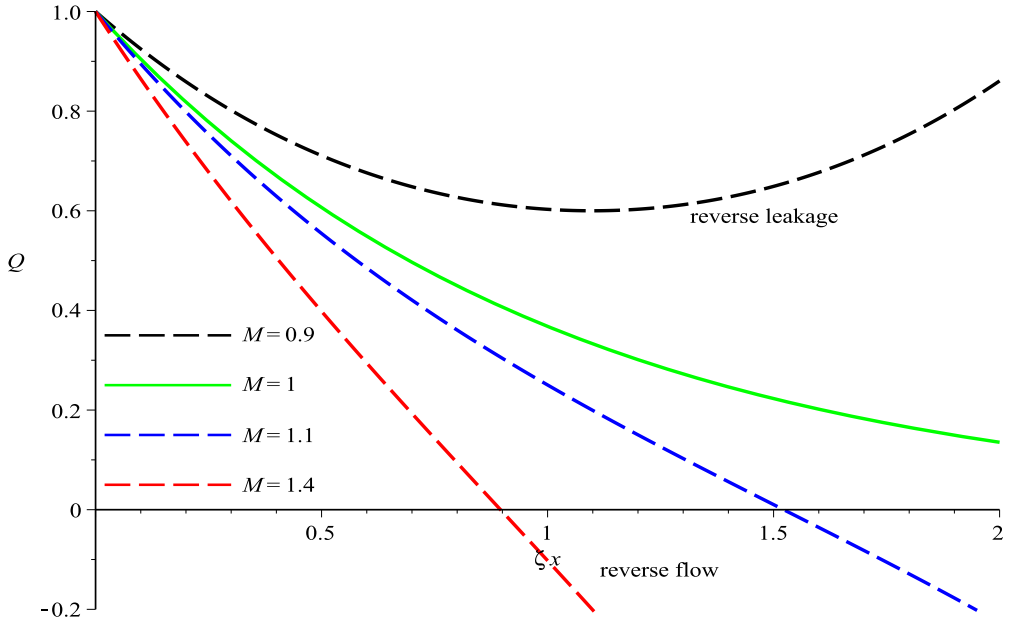

Figure 15. Variation of flow rate with M, $\lambda_3 = 7.5$.

hydraulic permeability as 2.41×10^{-11} cm^3/dynes s for the membrane having a thickness of 7.5×10^{-3} cm. When the viscosity of fluid was taken as 6.9×10^{-3} dynes s cm^{-2} from table 1, this yielded the value of L_p as 1.25×10^{-15} cm^2. The value of L_p calculated by the empirical results of Marshall *et al* [5] by using the experimental data of Kaufmann *et al* revealed that $Lp = 6.36 \times 10^{-16}$ cm^2. The experiments also showed that the mean axial pressure drop in the artificial kidney was about 15 mm Hg [5, 23]. Thus, a good agreement in the order of magnitudes of the ultrafiltration coefficient and mean pressure drop can be observed between the presented results and the earlier computed experimental and empirical results. This builds confidence in stating that the presented model can be used to obtain theoretical results in advance to study the hydrodynamical aspects of the flow in a FPH.

Data presented in table 1 and the estimated value of L_p reveal the dimensionless wall permeability (or filtration) parameter $K \ll 1$. Expanding (47) in power series of K, we have:

$$Q_U = 3\lambda_3\left(\frac{1}{2}\zeta^2 + 2\,p_i\,W\,K + O(K^2)\right). \tag{49}$$

Employing the dimensionless variables defined in equation (12), we obtain

$$\bar{Q}_U \approx 3\frac{\lambda_3\,A\,L_p}{\mu\,s}(\bar{p}_i - \bar{p}_m)\left[1 - \frac{3\,L^2\,\mu\,\bar{Q}_0}{2\,\lambda_1\,A\,a^3(\bar{p}_i - \bar{p}_m)}\right], \tag{50}$$

where $A = 2wL$ is used for membrane area. From this equation it is revealed that for those hemodialyzers in which

$$\frac{3\,L^2\,\mu\,\bar{Q}_0}{2\,\lambda_1\,A\,a^3(\bar{p}_i - \bar{p}_m)} \ll 1, \tag{51}$$

the ultrafiltration rate is given by:

$$\bar{Q}_U \approx 3\frac{\lambda_3\,A\,L_p}{\mu\,s}(\bar{p}_i - \bar{p}_m). \tag{52}$$

An inspection of equation (52) suggests that the ultrafiltration rate is directly proportional to the the dimensionless yield stress and wall slip parameter λ_3, mechanical filtration coefficient L_p and membrane area A, whereas, it is inversely proportional to the membrane thickness s and channel half width a. The linear dependence of $\bar{Q}_U$ on $\bar{p}_i\bar{p}_m$ has been found experimentally by Malino *et al* [33] and Mcdonald [34] and was suggested empirically by Marshall *et al* [5] and Lu *et al* [26]. A series of experiments performed by Brown *et al* [35] also highlighted the dependence of $\bar{Q}_U$ on the mechanical filtration coefficient, membrane thickness, and the membrane area.

Another important fact related to the renal tubular flow in kidneys can be observed from the expressions describing the mean pressure and flow rate, respectively in (38) and (33). These equations can be rewritten as:

$$P_M(x) = p_i\left(\cosh\zeta\,x - \frac{1}{M}\sinh\zeta\,x\right), \tag{53}$$

$$Q(x) = \frac{15}{2}\lambda_3(\cosh\zeta\,x - M\sinh\zeta\,x), \tag{54}$$

where $M = \dfrac{2\,p_i\,W\,K}{\zeta}$. A consideration of the right-hand sides of these equations suggests that the parameter M may influence the behavior of mean pressure and flow rate. Figure 15 is drawn to explore this fact for some values of M. This figure reveals that when $M > 1$, the flow rate started decaying from its maximum value one ($\bar{Q}_0$ in dimensional form), became zero at certain point, and then became negative as $\zeta\,x \to \infty$. Thus, a reverse flow situation arose when $M > 1$. For $M < 1$, $Q(x)$ decayed initially from $Q(0) = 1$, attained its minimum value at a point, and then started

increasing. This caused the reverse leakage phenomena for $\zeta < 1$. For $M = 1$, the graph of flow rate behaved as an exponentially-decaying function. An analogous discussion can also be made for the variation of mean pressure $P_M(x)$ with the parameter M.

The above discussion together with figure 15 reveal that for the creeping motion of a micropolar fluid in a porous-walled channel, in order to have no reverse flow and no reverse leakage, the value of parameter M must be approximately one. Substituting $M = 1$ in equation (54) yields

$$Q(x) = \frac{15}{2}\lambda_3 \exp(-\zeta\, x). \tag{55}$$

This is a well-accepted result regarding the flow rate of filtrate in the renal tubule of kidneys, which was empirically proven by Kellman [36] and used by many researchers in the study of fluid flow in a permeable tube with application to renal tubules of kidneys [3, 25, 37, 38].

8. Conclusions

We have presented the flow of a Casson fluid between two parallel permeable membranes with an application to the blood flow in a FPH. Governing equations of motion are exactly solved using the low Reynolds number and long membrane length assumption. It is found that the maximum values of axial and normal velocity components and the local wall shear stress for the Casson fluid are lesser than that of the Newtonian fluid, whereas the mean pressure drop for the Casson fluid has higher magnitude than the Newtonian fluid. Fluid seepage is seen to be enhanced, and hence the filtration process can be accelerated, by increasing the membrane permeability. In the application to flow in an FPH, theoretical values of the membrane filtration coefficient and mean pressure drop are computed as $5.35 \times 10^{-16}\,\mathrm{cm}^2$ and 10.39 mm Hg, respectively. These values are found to be in a reasonable agreement with the corresponding available empirical and experimental values in the literature. For limiting values of certain physical parameters, we note that that the axial flow rate of Casson fluid in an FPH decays at an exponential rate. This is a physically valid and widely admitted result, used by several researchers in studying the blood filtration process in renal tubules of mammalian kidneys. In the limiting case when the Casson fluid and slip parameters approaches to zero, the presented solutions reduced to the Newtonian fluid flow solutions in permeable membranes. It is concluded that a wide range of applications in physiology and engineering can be covered up by the present investigation.

Conflict of interest

Authors declare that they have no potential conflicts of interest.

ORCID iDs

Muhammad Kahshan https://orcid.org/0000-0001-6324-3884
Dianchen Lu https://orcid.org/0000-0001-6896-172X

References

[1] Voutchkov N 2012 *Desalination Engineering: Planning and Design* (New-York: McGraw Hill Professional) 0071777164, 9780071777162
[2] Macey R I 1963 Pressure flow patterns in a cylinder with reabsorbing walls *Bull. Math. Biophys.* **25** 303–12
[3] Macey R I 1965 Hydrodynamics in the renal tubule *Bull. Math. Biophys.* **27** 117–24
[4] Marshall E A and Trowbridge E A 1974 Flow of a newtonian fluid through a permeable tube: the application to the proximal renal tubule *Bull. Math. Biol.* **36** 457–76
[5] Marshall E A, Trowbridge E A and Aplin A J 1975 Flow of a newtonian fluid between parallel flat permeable plateshe application to a flat-plate hemodialyzer *Math. Biosci.* **27** 119–39
[6] Kozinski A A, Schmidt F P and Lightfoot E N 1970 Velocity profiles in porous-walled ducts *Ind. Eng. Chem. Fundam.* **9** 502–5
[7] Papanastasiou T C *et al* 1999 *Viscous Fluid Flow* (Florida: CRC Press LLC) 4409780849316067 - CAT# 1606
[8] Berman S 1953 Laminar flow in channels with porous walls *J. Appl. Phys.* **24** 1232–5
[9] Berman A S 1958 Laminar flow in an annulus with porous walls *J. Appl. Phys.* **29** 71–5
[10] Yuan S W and Finkelstein A B 1956 Laminar pipe flow with injection and suction through a porous wall *Trans. ASME* **78** 719–24
[11] Haroon T, Siddiqui A M and Shahzad A 2016 Creeping flow of viscous fluid through a proximal tubule with uniform reabsorption: a mathematical study *Appl. Math. Sci.* **10** 795–807
[12] Siddiqui A M, Haroon T and Shahzad A 2016 Hydrodynamics of viscous fluid through porous slit with linear absorption *Appl. Math. Mech.* **37** 361–78
[13] Tu J-W and Ho C-D 2010 Two-dimensional mass-transfer model of a flat-plate dialyzer with ultrafiltration operation *Chem. Eng. Technol.* **33** 1358–68
[14] Zeng Y, Yao X-H and Liu X-H 2014 Numerical simulation of the effect of permeability on the hydrodynamics in a parallel-plate coculture flow chamber *Comput. Meth. Biomech. Biomed. Eng.* **17** 875–87
[15] Chotard-Ghodsnia R, Drochon A and Grebe R 2002 A new flow chamber for the study of shear stress and transmural pressure upon cells adhering to a porous biomaterial *J. Biomech. Eng.* **124** 258–61
[16] Bird R B *et al* 1987 *Dynamics of Polymeric Liquids* Vol 1 (New York: Wiley) 672978-0-471-80245-7
[17] Cason N 1959 *Rheology of Disperse Systems* ed C C Mills (New York: Pergamon) pp 84–104
[18] Hayat T and Ali N 2008 Peristaltic motion of a jeffrey fluid under the effect of a magnetic field in a tube *Commun. Nonlinear Sci. Numer. Simul.* **13** 1343–52
[19] Beavers G S and Joseph D D 1967 Boundary conditions at a naturally permeable wall *J. Fluid Mech.* **30** 197–207
[20] Saffman P G 1971 On the boundary condition at the surface of a porous medium *Stud. Appl. Math.* **50** 93–101
[21] Darcy H P G 1856 Dètermination des lois daècoulement de laeau à travers le sable
[22] Drukker W, Parsons F M and Maher J F 2012 *Replacement of Renal Function by Dialysis: A Textbook of Dialysis*

(Netherlands: Springer Science & Business Media) (https://doi.org/10.1007/978-94-009-6768-7)
[23] Funck-Brentano J L, Sausse A, Vantelon J, Granger A, Zingraff J and Man N K 1969 A new disposable plate-kidney *Trans Am Soc Artif Intern Organs.* **15** 127–30
[24] Palatt P J, Sackin H and Tanner R I 1974 A hydrodynamic model of a permeable tubule *J. Theor. Biol.* **44** 287–303
[25] Siddiqui A M, Haroon T, Kahshan M and Iqbal M Z 2015 Slip effects on the flow of newtonian fluid in renal tubule *J. Comput. Theor. Nanosci.* **12** 4319–28
[26] Lu D, Kahshan M and Siddiqui A M 2019 Hydrodynamical study of micropolar fluid in a porous-walled channel: application to flat plate dialyzer *Symmetry* **11** 541
[27] Hayat T, Saleem N and Hendi A A 2011 A mathematical model for studying the slip effect on peristaltic motion with heat and mass transfer *Chin. Phys. Lett.* **28** 034702
[28] Tripathi D 2012 Peristaltic hemodynamic flow of couple-stress fluids through a porous medium with slip effect *Transp. Porous. Med.* **92** 559–72
[29] Pandey S K and Tripathi D 2010 Peristaltic transport of a casson fluid in a finite channel: application to flows of concentrated fluids in oesophagus *Int. J. Biomath.* **03** 453–72
[30] Das B and Batra R L 1995 Non-newtonian flow of blood in an arteriosclerotic blood vessel with rigid permeable walls *J. Theor. Biol.* **175** 1–11
[31] Pal D, Rudriah N and Devanathan R 1988 The effects of slip velocity at a membrane surface on blood flow in the microcirculation *J. Math. Biol.* **26** 705–12
[32] Kaufmann T G and Leonard E F 1968 Studies of intramembrane transport: a phenomenological approach *AlChE J.* **14** 110–7
[33] Malinow M R and Korzon W 1947 An experimental method for obtaining an ultrafiltrate of the blood *Transl. Res.* **32** 461–71
[34] McDonald H P Jr 1966 An automatic peritoneal dialysis machine: preliminary report *Trans Am Soc Artif Intern Organs.* **11** 83–5
[35] Brown H W and Schreiner G E 1962 Prolonged hemodialysis with bath refrigeration: the influence of dialyzer membrane thickness, temperature and other variables on performance *Trans. Am. Soc. Artif. Intern. Organs.* **8** 187–94
[36] Kelman R B 1962 A theoretical note on exponential flow in the proximal part of the mammalian nephron *Bull. Math. Biophys.* **24** 303–17
[37] Radhakrishnamacharya G, Chandra P and Kaimal M R 1981 A hydrodynamical study of the flow in renal tubules *Bull. Math. Biol.* **43** 151–63
[38] Siddiqui A M, Haroon T and Kahshan M 2015 Mhd flow of newtonian fluid in a permeable tubule *Magnetohydrodynamics* **51** 655–72